Journal of Materials Chemistry B

Check for updates

Trehalose-polyamine/DNA nanocomplexes: impact of vector architecture on cell and organ transfection selectivity†

Fernando Ortega-Caballero, [ID] [ab] María L. Santana-Armas, [c] Conchita Tros de Ilarduya, [ID] [c] Christophe Di Giorgio, [d] Raphäel Tripier, [ID] [e] Nathalie Le Bris, [ID] [e] Cedric Ollier, [ID] [e] Carmen Ortiz Mellet, [ID] [a] José M. García Fernández, [ID] [f] José L. Jiménez Blanco [ID] *[a] and Alejandro Méndez-Ardoy [ID] *[af]

A novel family of precision-engineered gene vectors with well-defined structures built on trehalose and trehalose-based macrocycles (cyclotrehalans) comprising linear or cyclic polyamine heads have been synthesized through procedures that exploit click chemistry reactions. The strategy was conceived to enable systematic structural variations and, at the same time, ensuring that enantiomerically pure vectors are obtained. Notably, changes in the molecular architecture translated into topological differences at the nanoscale upon co-assembly with plasmid DNA, especially regarding the presence of regions with short- or long-range internal order as observed by TEM. *In vitro* and *in vivo* experiments further evidenced a significant impact on cell and organ transfection selectivity. Altogether, the results highlight the potential of trehalose-polyamine/pDNA nanocomplex monoformulations to achieve targeting transfection without the need for any additional cell- or organ-sorting component.

Introduction

A range of new therapies relay on the safe delivery of nucleic acids into cells.[1,2] One of the main hurdles is developing carrier systems (vectors) with the ability to transport the therapeutic gene material with high efficiency and selectivity to the target site of action, avoiding off-target effects. While viruses are well-suited for this purpose, viral systems still bring concerns about immunogenicity, random integration in the host genome, limited DNA packaging capacity and the cost of clinical grade production of large batches.[3] Non-viral vector systems are an attractive alternative to bypass these issues.[4] Currently approved non-viral gene therapies include the siRNA drug Patisiran (Onpattro),[5] or the mRNA-based vaccines[6] that played an essential role in global prophylaxis during the SARS-COV-2 pandemic,[7] with a number of clinical trials ongoing.[8]

Most of the nonviral vectors commonly used in nucleic acid therapeutics are intrinsically polydisperse in nature (*e.g.*, cationic polymers),[9–11] lack conformational definition (*e.g.*, cationic dendrimers) and/or require multicomponent formulations (*e.g.* cationic lipids),[9] which represents a major limitation for conducting structure–activity relationship (SAR) studies in view of vector optimization.[12–15] Consequently, an urgent need remains in the field for well-defined molecular vectors susceptible to systematic chemical modifications through procedures warranting enantiomeric purity and well-suited for diversity-oriented schemes.[16–22] Molecular vectors fulfilling these postulates have become accessible by exploiting multifunctional platforms amenable to precision chemistry transformations.[23–28] Carbohydrate-based scaffolds have proven particularly useful for such endeavor. Most of the work in this area has focused on the realm of cyclodextrins. Their axial symmetry, neat face differentiation and distinct hydroxyl reactivity allow the installation of multivalent displays of functional elements for nucleic acid recognition (*i.e.*, cation ionizable groups and hydrogen-bonding centers) and self-organization (*e.g.*, lipid tails or aromatic modules) with precise relative orientations.[29–33]

[a] *Department of Organic Chemistry, Faculty of Chemistry, University of Seville, c/Profesor García González 1, Sevilla 41012, Spain. E-mail: jljb@us.es alejandroma@us.es*

[b] *Department of Organic Chemistry, Higher Polytechnic School, University of Seville, c/Virgen de África 7, Sevilla 41011, Spain*

[c] *Department of Pharmaceutical Sciences, School of Pharmacy and Nutrition, University of Navarra, Pamplona 31080, Spain*

[d] *Institut de Chimie Nice, UMR 7272, Université Côte d'Azur, 28 Avenue de Valrose, Nice 06108, France*

[e] *Université de Brest, UMR CNRS 6521 CEMCA, 6 Avenue Victor le Gorgeu, Brest 29238, France*

[f] *Instituto de Investigaciones Químicas (IIQ), CSIC –, Universidad de Sevilla, Avda. Américo Vespucio 49, Sevilla 41092, Spain*

† Electronic supplementary information (ESI) available. See DOI: https://doi.org/10.1039/d3tb02889e

This journal is © The Royal Society of Chemistry 2024

J. Mater. Chem. B, 2024, **12**, 3445–3452 | **3445**

Interestingly, such favorable features are shared by the C_2-symmetric disaccharide α,α'-trehalose. This was recently exploited to develop a novel family of gemini-type molecular vectors endowed with facial amphiphilicity, termed Siamese-twin surfactants that exhibited efficient DNA nanocomplexation and delivery *in vitro* and *in vivo*.[34] Further on, α,α'-trehalose-based macrocycles (cyclotrehalans, CTs) were found to undergo co-assembly with plasmid DNA (pDNA) to afford transfectious nanocomplexes (CTplexes) with organ-selective gene delivery capabilities.[35]

The ensemble of the reported results on trehalose-based non-viral vectors evidences a remarkable influence of molecular architecture on the topological characteristics of the resulting vector-DNA nanocomplexes. The latter in turn translates into distinct cell selectivity and tissue tropism in mice models, probably due to shape and surface property-differentiated physiological barrier escape properties.[36]

The possibility of imparting targeting abilities by molecular vector design, without the need for installing a biorecognizable ligand or the coformulation with a third component, opens new avenues in non-viral gene delivery that remain largely unexplored. In this work we probe the effect of different linear and cyclic arrangements of polyamine heads displayed on trehalose or on a dimeric cyclotrehalan (Fig. 1) in the pDNA complexation and the transfection outcome *in vitro* and *in vivo*. We keep in mind reported molecular modelling studies on linear polyamines[37–39] suggesting that their self-folding might hamper an optimal DNA complexation.[40] Cyclic polyamines, such as cyclen (1,4,7,10-tetraazacyclododecane) and

cyclam (1,4,8,11-tetraazacyclotetradecane), can mitigate this detrimental effect. Indeed, cyclen and cyclam have been proposed as delivery assistants after complexation with metallic cations, but less frequently as fundamental motifs to drive DNA binding.[41–50]

Results and discussion

Synthesis of trehalose and cyclotrehalan gene vectors

The collection of trehalose-polyamine vectors prepared in this work is depicted in Fig. 1. They were conceived to assess the effect of linear *versus* cyclic polyamine arrangements, amphiphilic *versus* non amphiphilic character, macrocyclic dimers *versus* monomeric trehalose scaffolds and thiourea *versus* 1,2,3-triazole connectors in their pDNA complexation and delivery properties. The radial polycationic derivative **1** was prepared as reported previously (Fig. 1).[32] The novel Janus-type amphiphilic derivatives **2–7** were accessed by "click" multiconjugation of cyclotrehalan or trehalose derivatives and suitably functionalized polyamine building blocks. Thus, a thiourea-forming reaction between cyclotrehalan hexaamine **8** and isothiocyanates **9** or **10** gave the corresponding Boc-protected adducts **11** and **12** (35% and 74% isolated yields). Subsequent acidic treatment afforded the target vectors **2** and **3** (Scheme 1). Similarly, the trehalose-cyclam thiourea conjugate **4** was obtained by coupling the trehalose diisothiocyanate **13** and the 2-aminoethyl cyclam derivative **14**[51] (→ **15**), followed by Boc-deprotection (61% yield, Scheme 2). The
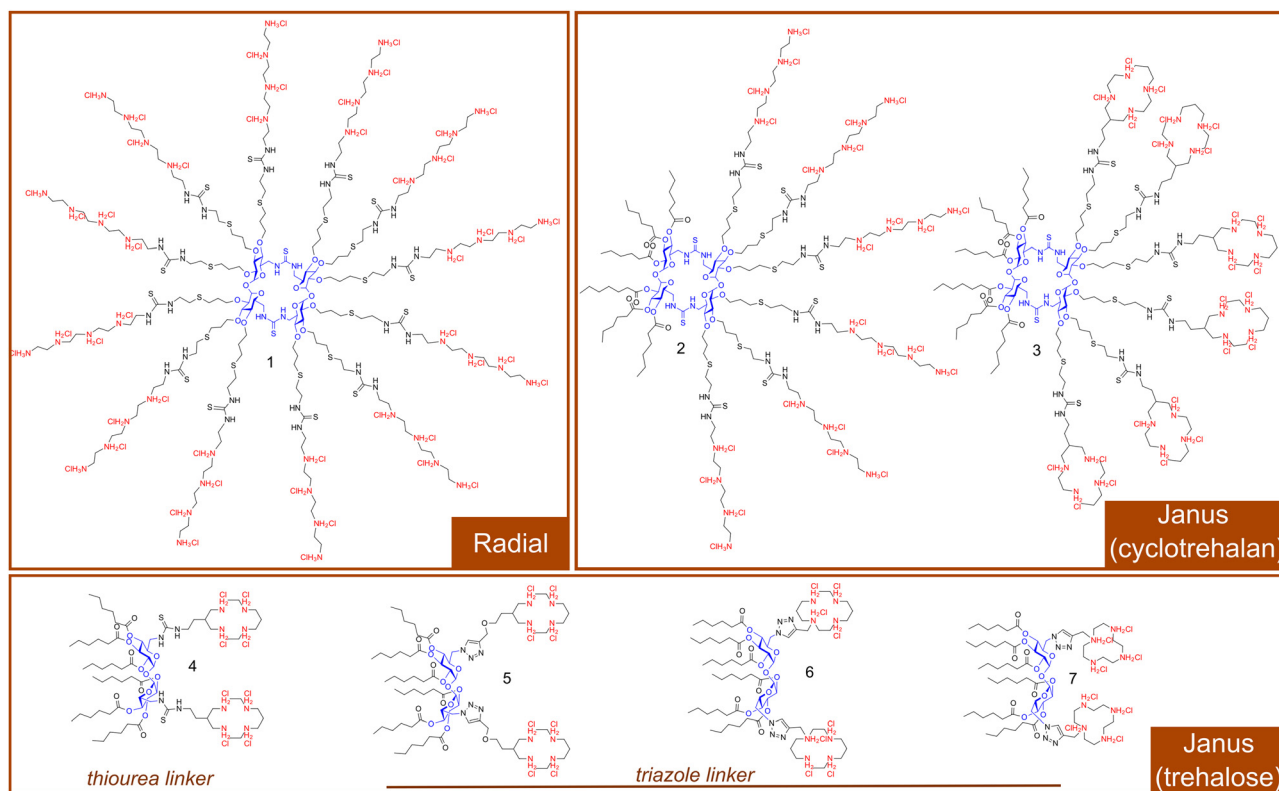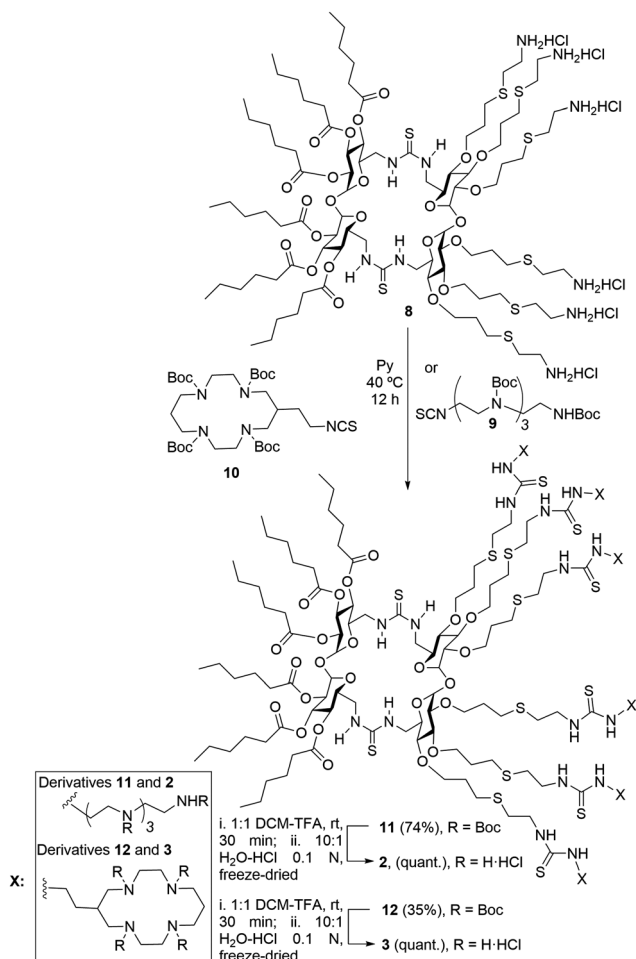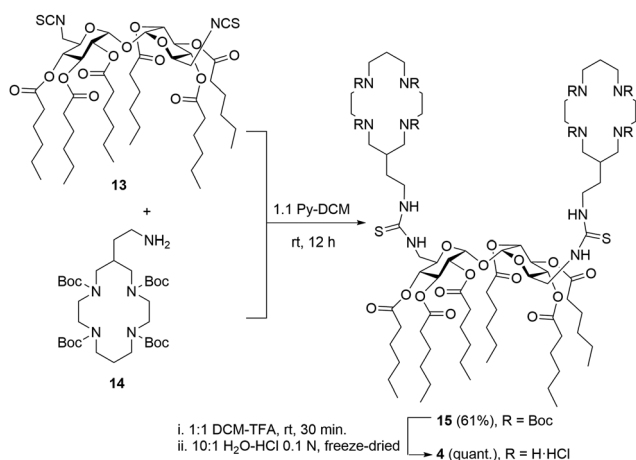

Fig. 1 Chemical structures of the trehalose-based molecular vector prototypes prepared and assayed in this work. All compounds **1–7** were isolated as the corresponding per-hydrochloride salts.

3446 | *J. Mater. Chem. B*, 2024, **12**, 3445–3452

This journal is © The Royal Society of Chemistry 2024

Scheme 1 Synthesis of Janus-amphiphilic cyclotrehalan-based vectors **2** and **3**.

Scheme 2 Synthesis of thiourea-linked trehalose-cyclam amphiphile **4**.

triazole-linked vectors **5–7** were prepared by Cu(ɪ)-catalyzed azide–alkyne coupling (CuAAC) between diazide **17** and alkynes **16–19** (→ **20-22**) using resin-linked Cu(ɪ)[52] in H$_2$O-^{t}BuOH and final carbamate hydrolysis (38–71%; Scheme 3). A refined synthesis for compound **5** has been autonomously developed within
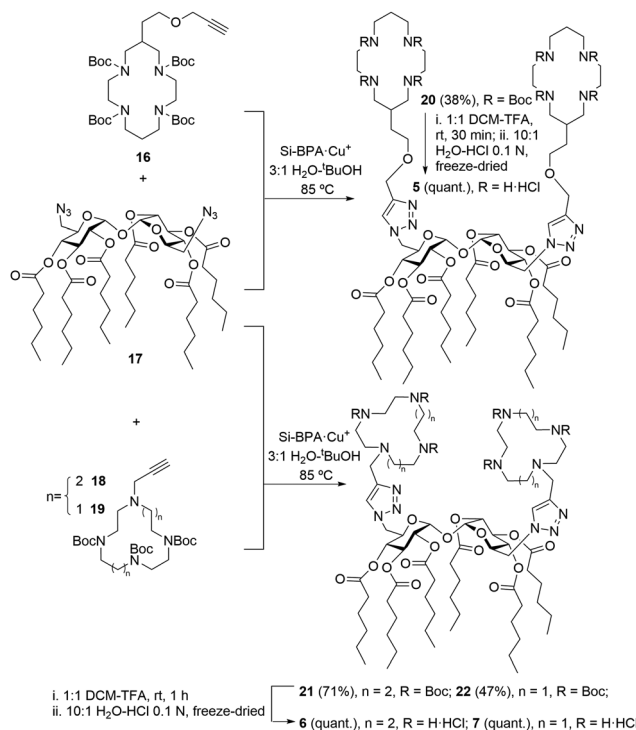
Scheme 3 Synthesis of triazole-linked cyclen/cyclam-trehalose amphiphiles **5–7**.

the framework of a distinct project; comprehensive details are presented in a parallel paper.[53]

pDNA complexation studies

In order to determine the pDNA complexation abilities of **1–7**, we mixed the vectors with a plasmid encoding luciferase (pCMV-Luc VR1216, 6934 bp) at different nitrogen (N) to phosphorous (P) stoichiometric ratios (N/P) in BHG buffer (HEPES 10 mM, pH 7.4, glucose 5% w/v). The pDNA protection efficacy and nano-particle characteristics (size, surface potential, and morphology) were determined by electrophoretic mobility shift assay (EMSA) in agarose gel, dynamic light scattering (DLS), ζ-potential mea-surements and transmission electron microscopy (TEM).

Gel retardation experiments using GelRed® as a visualiza-tion agent revealed that all vectors were able to inhibit DNA migration to positive potentials at N/P 10, therefore supporting that the negative charges of the DNA phosphate backbone are effectively screened by the vector cationic clusters. Except for **1**, pDNA staining is prevented in the presence of the vector, suggest-ing limited accessibility of the plasmid in the nanocomplex to the intercalating probe (Fig. 2a). To test the protection capabilities of the vectors towards enzymatic degradation, the nanocomplexes were incubated in the presence of DNAse, then treated with sodium dodecylsulfate (SDS) to provoke disruption and pDNA release and tested by EMSA (Fig. 2b). pDNA degradation results in total fading of the fluorescence bands in the gel, as observed for the control.

The relatively weak fluorescence intensity in the case of complexes prepared from the cationic vector **1** points to
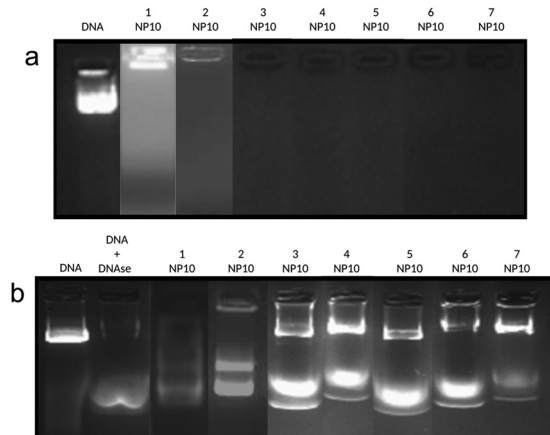
This journal is © The Royal Society of Chemistry 2024

J. Mater. Chem. B, 2024, **12**, 3445–3452 | **3447**

Fig. 2 Agarose gel electrophoresis EMSA gels for nanocomplexes formulated with pDNA (pCMV-Luc VR1216) and compounds **1–7** at N/P 10 (HEPES 10 mM, pH 7.4, glucose 5% w/v), before (a) and after treatment with DNase and subsequent dissociation of the complexes with sodium dodecylsulfate (b); naked pDNA was used as a control and GelRed® as a stainer.

incomplete protection. On the other hand, complexes prepared from **3–7** showed the presence of both pristine DNA and partially degraded DNA. This indicates that the protection abilities of vectors **3–7** were superior to those of **1–2**.

The nanoparticle size distribution and surface charge were determined in solution by DLS measurements. The hydrodynamic diameter (D_h) values and ζ-potential of the formulations at N/P 10 and 20 are shown in Table 1.

The D_h values ranged from 90 to 173 nm, and surface charges were positive in all cases, ranging from +13 to +25 mV. Generally, the higher the N/P ratio, the smaller the nanoparticle size, which is compatible with a larger fraction of phosphates screened by the protonated amines. The incorporation of cyclic polyamines (*e.g.* **2** *vs.* **3**) had a positive impact on the ability of the vectors to generate smaller nanoparticles. In addition, the use of the thiourea linkers (*e.g.* **4** *vs.* **5** and **6**) also yielded smaller nanoparticles, suggesting that the cationic and hydrogen bond donor centers are optimally arranged to promote pDNA condensation upon co-assembly. At higher N/P ratios (20), cyclotrehalan-based DNA complexes (**2** and **3**) showed generally smaller hydrodynamic diameters than complexes prepared with
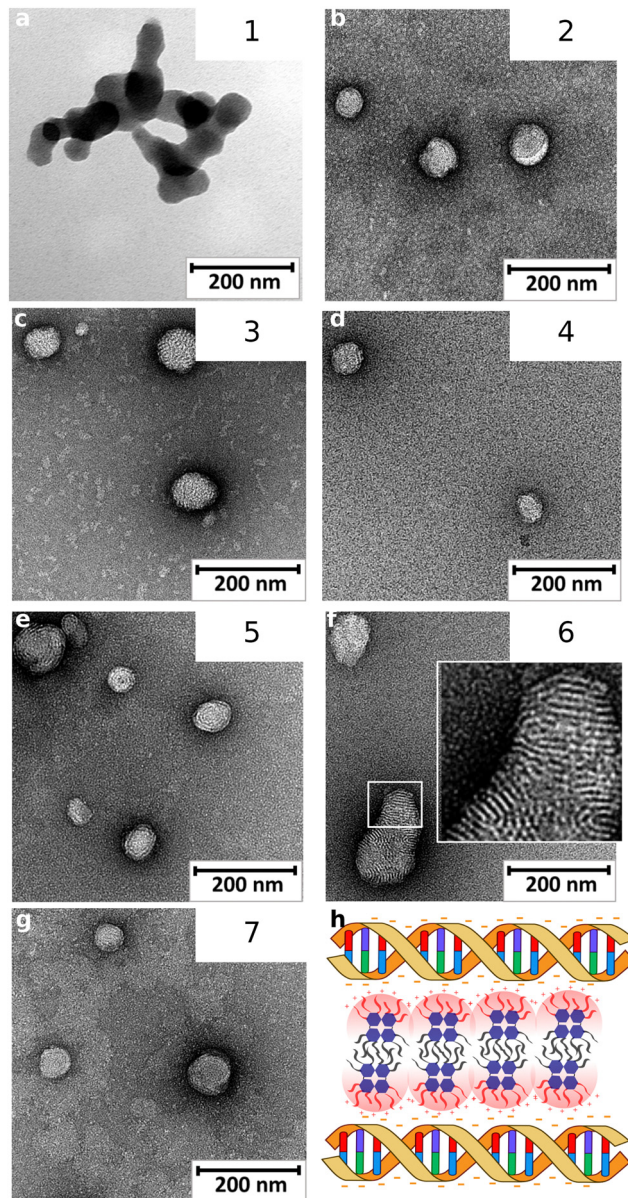
Table 1 Hydrodynamic diameters (D_h) and ζ-potentials (DLS) for the nanocomplexes formulated with the polycation trehalose derivatives and pDNA (pCMV-Luc VR1216) at N/P 10 and 20 in BHG (HEPES 10 mM, pH 7.4, glucose 5% w/v)

| Vector | N/P 10 | | N/P 20 | |
	D_h (nm)	ζ-potential (mV)	Size (nm)	ζ-potential (mV)
1[a]	133 ± 6	+24 ± 3	107 ± 6	+25 ± 1
2	166 ± 1	+17 ± 2	103 ± 3	+18 ± 1
3	111 ± 9	+21 ± 1	91 ± 3	+16 ± 3
4	101 ± 11	+19 ± 5	90 ± 2	+13 ± 1
5	157 ± 12	+10 ± 5	122 ± 26	+25 ± 10
6	173 ± 4	+20 ± 4	139 ± 7	+24 ± 5
7	161 ± 9	+12 ± 3	132 ± 5	+21 ± 5

[a] Data are from ref. 32 and are here included for comparative purposes.

Fig. 3 Representative TEM micrographs of the DNA–vector complexes at N/P 20 in HEPES 20 mM, pH 7.4, DNA 303 μM phosphate.

trehalose derivatives **4**, **5**, **6** and **7** (91–103 nm *vs.* 90–139 nm). This could be related to entropic effects arising from the multivalent exposure of a higher number of cationic arms in the cyclotrehalan-based vectors.

The morphology of the nanocomplexes was investigated by TEM after uranyl acetate staining (Fig. 3).

The non-amphiphilic derivative **1** (Fig. 3a and Fig. S1, ESI†) co-assembled with pDNA into networked blobs of about 200 nm with no observable internal structure. Differently, the micrographs of the nanocomplexes formulated from the amphiphilic vectors **2–7** showed well-defined quasi-spherical or pear-shaped nanoparticles with different ultrathin organizations. Thus, for compounds **2**, **5** and **7** onion-like long-range multilamellar arrangements of dark (high electron density) and light regions

3448 | *J. Mater. Chem. B*, 2024, **12**, 3445–3452

This journal is © The Royal Society of Chemistry 2024

are apparent (Fig. 3b, e, and g and Fig. S1, ESI†), in agreement with alternate dispositions of pDNA and cationic lipid bilayers (Fig. 3h and Fig. S1, ESI†).[30] Nanocomplexes obtained from **3** and **4** also showed alternating dark and light regions, but in a highly sinusoidal short-range arrangement with multiple arcs (Fig. 3c, d and Fig. S1, ESI†). Compound **6** nanocomplexes had mixed characteristics, with areas displaying long- and short-range order (Fig. 3f and Fig. S1, ESI†).

In vitro gene delivery and toxicity studies

The pDNA delivery efficiencies of vectors **1–7** were first evaluated *in vitro* in African green monkey kidney fibroblast (COS-7), human cervix cancer (HeLa), human cellular hepatocarcinoma (HepG2) and mouse ascites macrophage (RAW264.7) cells. After 4 h incubation, the medium was replaced and the cells were incubated for 48 h, then lysed and the luciferase expression measured and standardised against the total amount of protein per well. The results are shown in Fig. 4.
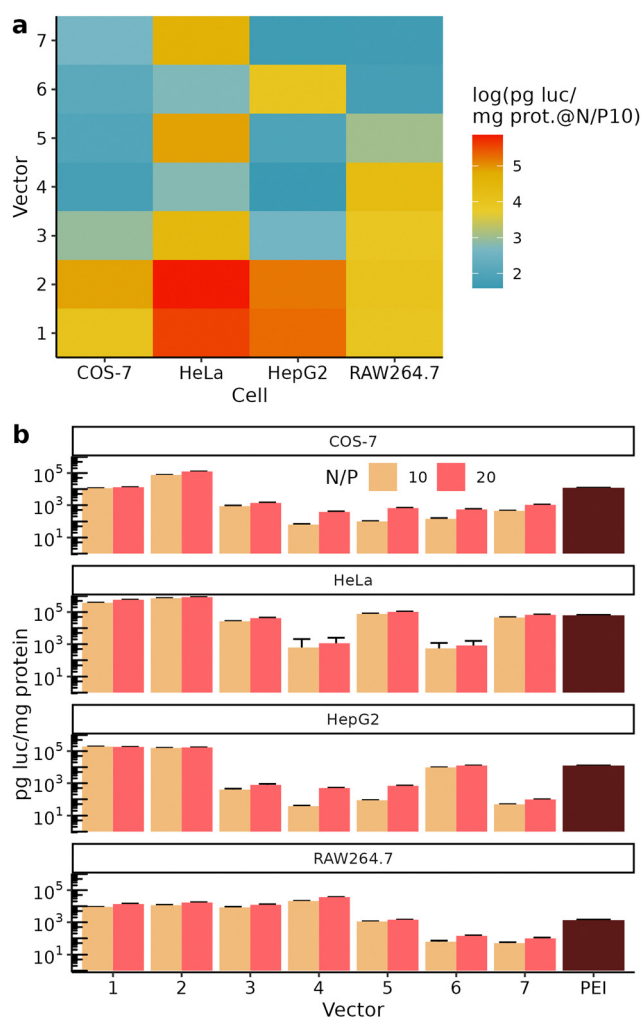

Fig. 4 Transfection efficiency of vectors in COS-7, HeLa, HepG2 and RAW264.7 cells: (a) heatmap comparing transfection efficiency at N/P 10; (b) transfection efficiency at N/P 10 and 20 in BHG (HEPES 10 mM, pH 7.4, glucose 5% w/v). PEI is used as a positive transfection control at N/P 10. Bars denote the standard deviation.

In general, increasing the N/P ratio from 10 to 20 led to higher transfection levels (Fig. 4b), though at the expense of a toxicity penalty (see below). The tetraethyleneimine-decorated vectors showed the highest efficacy across all cell lines, overpassing poly(ethyleneimine)-formulated polyplexes (N/P 10) used as a positive control (Fig. 4b). They behave as broad range transfection agents, performing especially well in HeLa and HepG2 cells. Trehalose-cyclam and -cyclen-based vectors generally reached lower expression levels but displayed higher cell selectivity. Thus, compounds **3** and **4** mediated transfection preferentially in RAW264.7 cells, **5** and **7** in HeLa cells and **6** in HepG2, while they all lacked substantial expression levels in COS-7 cells. Ascribing these differences in relative cell transfection performances to the above commented dissimilarities in the internal order in the corresponding nanocomplexes is appealing. Indeed, a direct relationship between the presence of short-range order, long-range order, or mixed areas, in the nanocomplexes and the transfection outcome can be drawn. Such generalization must be taken with care, however. The diversity of transfection efficiency across cell lines can reflect intrinsic differences in endocytic processes or endosomal escape mechanisms that depend on an ensemble of cell and vector factor.[52]

Toxicity of the formulations prepared in this work was assessed by the MTT assay. The data revealed low toxicity in all cases (Fig. S2, ESI†). At N/P 10, cell viabilities were above 90%. Increasing the N/P ratio to 20 led to an increase in toxicity. Nevertheless, it remained above 80% with an average cell viability of 90%. Anyway, all formulations with the synthesized vectors display lower toxicity than PEI polyplexes (50–75% cell viability across the different cell lines; ESI,† Fig. S2).

In vivo gene delivery

The *in vivo* delivery efficiency was evaluated after systemic injection of the nanocomplexes prepared at N/P 10 (HEPES 10 mM, pH 7.4, glucose 5% w/v) in the mouse tail vein. All experiments were carried out according to ethical guidelines established by Directive 86/609/EEC-RD 53/2013 February 1, and with the approval of the Committee on Animal Research at the University of Navarra (number of protocol 017-19). Twenty-four hours after injection the mice were sacrificed, and the luciferase expression measured in heart, kidneys, liver, lungs, and spleen (Fig. 5). Surprisingly, the formulation obtained from the non-amphiphilic derivative **1** showed negligible luciferase levels in all organs. This could arise from aggregation leading to premature clearance or because of degradation due to inefficient cargo protection, according to the EMSA data. On the opposite, compound **2** promoted substantial luciferase expression in all organs, with higher expression levels in the lungs and the liver. Paralleling the *in vitro* results, cyclam and cyclen derivatives **3–7** revealed a lower total expression of luciferase but a higher selectivity towards specific organs. Hence, vectors **3**, **4** and **6** showed preferential expression in the lungs, the spleen, and the liver, respectively, whereas vectors **5** and **7** showed a marked tropism to the kidney (Fig. 5a and b).

The data evidence a clear advantage of amphiphilic over non-amphiphilic molecular vectors for *in vivo* applications.
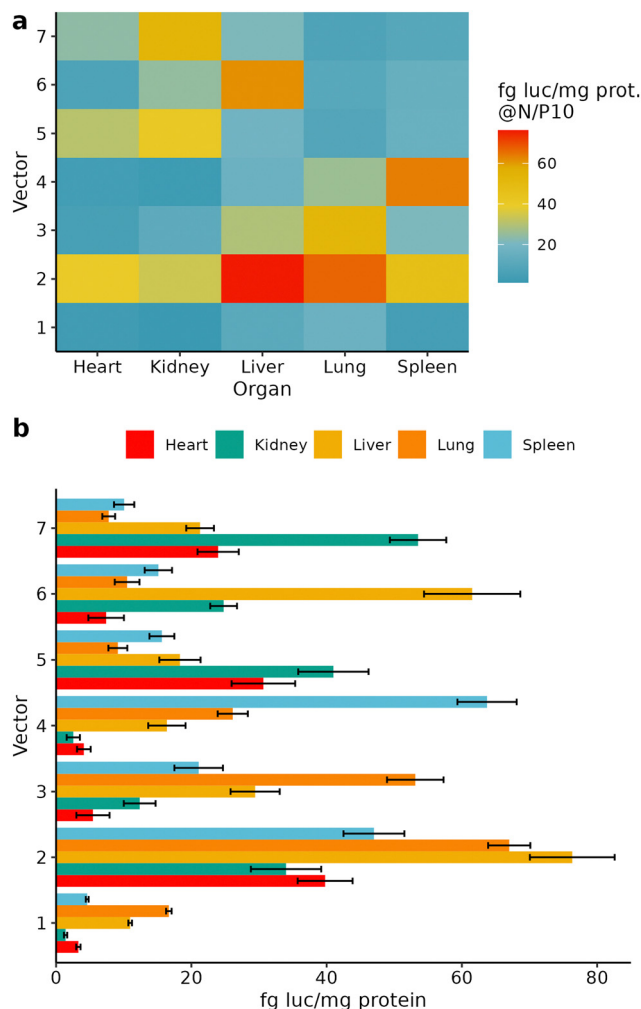
This journal is © The Royal Society of Chemistry 2024

J. Mater. Chem. B, 2024, **12**, 3445–3452 | **3449**

Fig. 5 *In vivo* luciferase expression after systemic injection in mice models. Luciferase expression was standardized against total protein; (a) comparative heatmap. (b) Column plot. Bars indicate standard deviation.

They also support that restricting the flexibility of the cationic centres by using cyclic instead of linear polyamines as cationic heads enhances organ selectivity. This effect can only in part be rationalized in terms of the impact of changes at the molecular level on the organizational patterns at the nanoscale.

Other molecular and supramolecular features may be responsible for such observations. For instance, compounds **2**, **3** and **4**, the three forming spherical nanocomplexes with onion-line multilamellar internal structures, show a differential organ selectivity. Thus, polyethyleneimine amphiphile **2** behaves as a broad-range organ selective vector with preference towards liver and lungs. In contrast, cyclam derivatives **3** and **4** are more selective and exhibit differential preference for the lungs and the spleen, respectively. Nanocomplexes prepared from **5** and **7**, which exhibit a characteristic sinusoidal internal structure, both transfect preferentially the kidney, but the cyclen derivative **7** is significantly more selective than the cyclam analogue **5**. Finally, the enhanced tropism of **6** towards the liver as compared with **2** might be due to the partial loss long-range order of the corresponding nanocomplexes.

Conclusions

A novel collection of structurally defined gene delivery systems with varied molecular architectures have been prepared from trehalose and linear or cyclic polyamine precursors by a synthetic strategy based on click chemistry multiconjugation reactions. Co-formulation with pDNA rendered self-assembled transfectious nanocomplexes with topological characteristics and internal organizational patterns that are strongly dependent on the molecular features of the vector. A comparative evaluation of the *in vitro* and *in vivo* transfection capabilities evidenced remarkable increases in cell and organ selectivity for compounds bearing cyclic polyamine-type cationic heads. Depending on the overall architecture, different cells and organs could be targeted without the need for involving any biorecognition component. Collectively, these results reinforce the notion that subtle differences in the molecular vector design can have a meaningful impact at the nanoscale and strongly influence the ability of the resulting nanocomplexes to cross biological barriers. They further reveal a new strategy to finely customize the vector in order to program a precise destination in biological environments. Finally, they warrant additional investigations on molecular gene vector structure-nanocomplex property-transfection efficiency relationships in view of realizing the goal of ligand-free site-specific nucleic acid therapeutics.

Author contributions

F. Ortega Caballero: investigation, supervision and writing-review & editing. María L. Santana-Armas: investigation. C. Tros de Ilarduya: investigation, Christophe Di Giorgio: investigation. Raphäel Tripier: resources. Nathalie Le Bris: investigation, resources. Cedric Ollier: investigation. C. Ortiz Mellet: project administration, funding acquisition and writing-review & editing. J. M. García Fernández: conceptualization, project administration and writing-review & editing. J. L. Jiménez Blanco: supervision, investigation and writing – original draft. Alejandro Méndez-Ardoy: investigation, writing – original draft.

Conflicts of interest

There are no conflicts to declare.

Acknowledgements

3450 | *J. Mater. Chem. B,* 2024, **12**, 3445–3452

This journal is © The Royal Society of Chemistry 2024

Notes and references

1 B. B. Mendes, J. Conniot, A. Avital, D. Yao, X. Jiang, X. Zhou, N. Sharf-Pauker, Y. Xiao, O. Adir, H. Liang, J. Shi, A. Schroeder and J. Conde, *Nat. Rev. Methods Primers*, 2022, **2**, 24.

2 A. Gupta, J. L. Andresen, R. S. Manan and R. Langer, *Adv. Drug Delivery Rev.*, 2021, **178**, 113834.

3 K. Kaygisiz and C. V. Synatschke, *Biomater. Sci.*, 2020, **8**, 6113–6156.

4 I. Lostalé-Seijo and J. Montenegro, *Nat. Rev. Chem.*, 2018, **2**, 258–277.

5 E. A. Narasipura, R. VanKeulen-Miller, Y. Ma and O. S. Fenton, *Bioconjugate Chem.*, 2023, **34**, 1177–1197.

6 U. Sahin, K. Karikó and Ö. Türeci, *Nat. Rev. Drug Discovery*, 2014, **13**, 759–780.

7 M. D. Shin, S. Shukla, Y. H. Chung, V. Beiss, S. K. Chan, O. A. Ortega-Rivera, D. M. Wirth, A. Chen, M. Sack, J. K. Pokorski and N. F. Steinmetz, *Nat. Nanotechnol.*, 2020, **15**, 646–655.

8 C. Chen, Z. Yang and X. Tang, *Med. Res. Rev.*, 2018, **38**, 829–869.

9 I. S. Pinto, R. A. Cordeiro and H. Faneca, *J. Controlled Release*, 2023, **353**, 196–215.

10 T. T. Smith, S. B. Stephan, H. F. Moffett, L. E. McKnight, W. Ji, D. Reiman, E. Bonagofski, M. E. Wohlfahrt, S. P. S. Pillai and M. T. Stephan, *Nat. Nanotechnol.*, 2017, **12**, 813–820.

11 J. M. Priegue, D. N. Crisan, J. Martínez-Costas, J. R. Granja, F. Fernandez-Trillo and J. Montenegro, *Angew. Chem., Int. Ed.*, 2016, **55**, 7492–7495.

12 P. Huang, H. Deng, Y. Zhou and X. Chen, *Matter*, 2022, **5**, 1670–1699.

13 Z. P. Tolstyka, H. Phillips, M. Cortez, Y. Wu, N. Ingle, J. B. Bell, P. B. Hackett and T. M. Reineke, *ACS Biomater. Sci. Eng.*, 2015, **2**, 43–55.

14 A. Sizovs, L. Xue, Z. P. Tolstyka, N. P. Ingle, Y. Wu, M. Cortez and T. M. Reineke, *J. Am. Chem. Soc.*, 2013, **135**, 15417–15424.

15 W. S. Boyle, K. Senger, J. Tolar and T. M. Reineke, *Biomacromolecules*, 2016, **18**, 56–67.

16 X. Zhao, J. Chen, M. Qiu, Y. Li, Z. Glass and Q. Xu, *Angew. Chem., Int. Ed.*, 2020, **59**, 20083–20089.

17 M. Qiu, Y. Li, H. Bloomer and Q. Xu, *Acc. Chem. Res.*, 2021, **54**, 4001–4011.

18 L. Miao, L. Li, Y. Huang, D. Delcassian, J. Chahal, J. Han, Y. Shi, K. Sadtler, W. Gao, J. Lin, J. C. Doloff, R. Langer and D. G. Anderson, *Nat. Biotechnol.*, 2019, **37**, 1174–1185.

19 K. A. Hajj, R. L. Ball, S. B. Deluty, S. R. Singh, D. Strelkova, C. M. Knapp and K. A. Whitehead, *Small*, 2019, **15**, 1805097.

20 I. Louzao, R. García-Fandiño and J. Montenegro, *J. Mater. Chem. B*, 2017, **5**, 4426–4434.

21 K. A. Whitehead, J. R. Dorkin, A. J. Vegas, P. H. Chang, O. Veiseh, J. Matthews, O. S. Fenton, Y. Zhang, K. T. Olejnik, V. Yesilyurt, D. Chen, S. Barros, B. Klebanov, T. Novobrantseva, R. Langer and D. G. Anderson, *Nat. Commun.*, 2014, **5**, 4277.

22 C. Gehin, J. Montenegro, E.-K. Bang, A. Cajaraville, S. Takayama, H. Hirose, S. Futaki, S. Matile and H. Riezman, *J. Am. Chem. Soc.*, 2013, **135**, 9295–9298.

23 L. Gallego-Yerga, I. Posadas, C. de la Torre, J. Ruiz-Almansa, F. Sansone, C. Ortiz Mellet, A. Casnati, J. M. García Fernández and V. Ceña, *Front. Pharmacol.*, 2017, **8**, 249.

24 J. Gasparello, M. Lomazzi, C. Papi, E. D'Aversa, F. Sansone, A. Casnati, G. Donofrío, R. Gambari and A. Finotti, *Mol. Ther.–Nucleic Acids*, 2019, **18**, 748–763.

25 L. Gallego-Yerga, J. M. Benito, L. Blanco-Fernández, M. Martínez-Negro, I. Vélaz, E. Aicart, E. Junquera, C. Ortiz Mellet, C. Trosde Ilarduya and J. M. García Fernández, *Chem. – Eur. J.*, 2018, **24**, 3825–3835.

26 D. Manzanares, I. Araya-Durán, L. Gallego-Yerga, P. Játiva, V. Márquez-Miranda, J. Canan, J. L. Jiménez Blanco, C. O. Mellet, F. D. González-Nilo, J. M. García Fernández and V. Ceña, *Nanomedicine*, 2017, **12**, 1607–1621.

27 W.-B. Zhang, X. Yu, C.-L. Wang, H.-J. Sun, I.-F. Hsieh, Y. Li, X.-H. Dong, K. Yue, R. Van Horn and S. Z. D. Cheng, *Macromolecules*, 2014, **47**, 1221–1239.

28 J. L. Jiménez Blanco, J. M. Benito, C. Ortiz Mellet and J. M. García Fernández, *J. Drug Delivery Sci. Technol.*, 2017, **42**, 18–37.

29 F. Ortega-Caballero, C. Ortiz Mellet, L. Le Gourriérec, N. Guilloteau, C. Di Giorgio, P. Vierling, J. Defaye and J. M. García Fernández, *Org. Lett.*, 2008, **10**, 5143–5146.

30 A. Díaz-Moscoso, L. L. Gourriérec, M. Gómez-García, J. M. Benito, P. Balbuena, F. Ortega-Caballero, N. Guilloteau, C. D. Giorgio, P. Vierling, J. Defaye, C. Ortiz Mellet and J. M. García Fernández, *Chem. – Eur. J.*, 2009, **15**, 12871–12888.

31 C. Ortiz Mellet, J. M. Benito and J. M. García Fernández, *Chem. – Eur. J.*, 2010, **16**, 6728–6742.

32 A. I. Carbajo-Gordillo, J. López-Fernández, J. M. Benito, J. L. Jiménez Blanco, M. L. Santana-Armas, G. Marcelo, C. Di Giorgio, C. Przybylski, C. Ortiz Mellet, C. Tros de Ilarduya, F. Mendicuti and J. M. García Fernández, *Macromol. Rapid Commun.*, 2022, **43**, 2200145.

33 A. I. Carbajo-Gordillo, J. L. Jiménez Blanco, J. M. Benito, H. Lana, G. Marcelo, C. Di Giorgio, C. Przybylski, H. Hinou, V. Ceña and C. Ortiz Mellet, *et al.*, *Biomacromolecules*, 2020, **21**, 5173–5188.

34 A. I. Carbajo-Gordillo, J. Rodríguez-Lavado, J. L. Jiménez Blanco, J. M. Benito, C. Di Giorgio, I. Vélaz, C. Tros de Ilarduya, C. Ortiz Mellet and J. M. García Fernández, *Chem. Commun.*, 2019, **55**, 8227–8230.

35 A. I. Carbajo-Gordillo, M. González-Cuesta, J. L. Jiménez Blanco, J. M. Benito, M. L. Santana-Armas, T. Carmona, C. Di Giorgio, C. Przybylski, C. Ortiz Mellet and C. Tros de Ilarduya, *Chem. – Eur. J.*, 2021, **27**, 9429–9438.

36 E. Blanco, H. Shen and M. Ferrari, *Nat. Biotechnol.*, 2015, **33**, 941–951.

37 X. Zhou, L. Xu, J. Xu, J. Wu, T. B. Kirk, D. Ma and W. Xue, *ACS Appl. Mater. Interfaces*, 2018, **10**, 35812–35829.

38 C. Xu, B. Yu, Y. Qi, N. Zhao and F. Xu, *Adv. Healthcare Mater.*, 2021, **10**, 2001183.

39 Y. J. Ooi, Y. Wen, J. Zhu, X. Song and J. Li, *Biomacromolecules*, 2020, **21**, 1136–1148.

This journal is © The Royal Society of Chemistry 2024

J. Mater. Chem. B, 2024, **12**, 3445–3452 | **3451**

40 T. Fujiwara, S. Hasegawa, N. Hirashima, M. Nakanishi and T. Ohwada, *Biochim. Biophys. Acta, Biomembr.*, 2000, **1468**, 396–402.

41 R.-M. Zhao, Y. Guo, H.-Z. Yang, J. Zhang and X.-Q. Yu, *New J. Chem.*, 2021, **45**, 13549–13557.

42 Y. Zhang, C.-Y. Li, J. Zhang, W.-J. Yi and X.-Q. Yu, *Chem. Biodiversity*, 2014, **11**, 233–244.

43 Q. Liu, Q.-Q. Jiang, W.-J. Yi, J. Zhang, X.-C. Zhang, M.-B. Wu, Y.-M. Zhang, W. Zhu and X.-Q. Yu, *Bioorg. Med. Chem.*, 2013, **21**, 3105–3113.

44 J. Li, Y. Zhu, S. T. Hazeldine, S. M. Firestine and D. Oupický, *Biomacromolecules*, 2012, **13**, 3220–3227.

45 Q.-D. Huang, J. Ren, H. Chen, W.-J. Ou, J. Zhang, Y. Fu, W. Zhu and X.-Q. Yu, *ChemPlusChem*, 2012, **77**, 584–591.

46 Z. Huang, Y.-P. Xiao, Y. Guo, H.-Z. Yang, R.-M. Zhao, J. Zhang and X.-Q. Yu, *Eur. Polym. J.*, 2022, **170**, 111153.

47 Q.-D. Huang, J. Ren, W.-J. Ou, Y. Fu, M.-Q. Cai, J. Zhang, W. Zhu and X.-Q. Yu, *Chem. Biol. Drug Des.*, 2012, **79**, 879–887.

48 Q.-D. Huang, W.-J. Ou, H. Chen, Z.-H. Feng, J.-Y. Wang, J. Zhang, W. Zhu and X.-Q. Yu, *Eur. J. Pharm. Biopharm.*, 2011, **78**, 326–335.

49 Y. Guo, J.-J. Chen, H.-Z. Yang, J. Zhang, R.-M. Zhao, Z. Huang and X.-Q. Yu, *ACS Appl. Bio Mater.*, 2020, **4**, 844–852.

50 Z. Chen, S. Liu, W. Liu, P. Jiang, L. Wang, J. Li, H. Zhou and T. Guo, *ACS Biomater. Sci. Eng.*, 2021, **7**, 5678–5689.

51 A. Megia-Fernandez, M. Ortega-Muñoz, J. Lopez-Jaramillo, F. Hernandez-Mateo and F. Santoyo-Gonzalez, *Adv. Synth. Catal.*, 2010, **352**, 3306–3320.

52 S. A. Smith, L. I. Selby, A. P. R. Johnston and G. K. Such, *Bioconjugate Chem.*, 2019, **30**, 263–272.

53 C. Ollier, A. Méndez-Ardoy, F. Ortega-Caballero, J. L. Jiménez Blanco, N. Le Bris and R. Tripier, *ChemRxiv.*, 2023, preprint, DOI: **10.26434/chemrxiv-2023-85pk4**.

3452 | *J. Mater. Chem. B*, 2024, **12**, 3445–3452

This journal is © The Royal Society of Chemistry 2024